J Appl Electrochem (2013) 43:583–593
DOI 10.1007/s10800-013-0543-4

ORIGINAL PAPER

Synthesis and optimization of NASICON-type $Li_3V_2(PO_4)_3$ by adipic acid-mediated solid-state approach

J. N. Son · S. H. Kim · M. C. Kim · K. J. Kim · V. Aravindan · W. I. Cho · Y. S. Lee

Received: 21 January 2013 / Accepted: 4 April 2013 / Published online: 12 April 2013

Abstract We report the synthesis and optimization of NASICON-type carbon-coated $Li_3V_2(PO_4)_3$ by solid-state approach. Adipic acid (AA) is used as the source material for the carbon. Initially, the synthesis of monoclinic $Li_3V_2(PO_4)_3$ is optimized at a precalcination temperature of 300 °C for 4 h and 900 °C for 8 h under Ar flow to yield a single phase. Powder characterizations such as thermogravimetric–differential thermal analysis, X-ray diffraction, scanning electron microscopy, transmission electron microscopy, and particle size distribution are conducted, and the results are presented. The AA concentration is varied according to the total metal ion composition in the compound (0.05, 0.1, and 0.15 M). Electrochemical Li-insertion properties are evaluated in half-cell configurations between 3 and 4.8 V vs. Li at a current density of 0.1 mA cm^{-2} at room temperature. Compared with the lower AA concentrations, Li/$Li_3V_2(PO_4)_3$ (0.15 M AA) cell exhibited discharge capacities of 178 and 147 mAh g^{-1} for the 1st and 50th cycles, respectively, and a capacity retention of 83 % after 50 cycles, which is 11 % higher than that of the native compound. Li/$Li_3V_2(PO_4)_3$ (0.15 M AA) showed better rate performances and delivered discharge capacities of 173, 165, 150, 132, 105, and 76 mAh g^{-1} at rates of 0.1, 0.2, 0.5, 1, 5, and 12 C, respectively. Electrochemical impedance spectroscopy reveals the enhancement in electronic conductivity profile after carbon coating.

Keywords NASICON · $Li_3V_2(PO_4)_3$ · Carbon coating · Adipic acid · Lithium battery

J. N. Son · S. H. Kim · M. C. Kim · K. J. Kim · V. Aravindan · Y. S. Lee (✉)
Faculty of Applied Chemical Engineering, Chonnam National University, Gwang-ju 500-757, South Korea
e-mail: leeys@chonnam.ac.kr

V. Aravindan
Energy Research Institute (ERI@N), Nanyang Technological University, Research Techno Plaza, 50 Nanyang Drive, Singapore 637553, Singapore

W. I. Cho
Energy and Environment Division, Korea Institute of Science and Technology, Seoul 136-791, South Korea

1 Introduction

Recently, Na^+ superionic conductor (NASICON)-type insertion hosts have attracted attention as prospective electrode materials for lithium-ion batteries (LIBs) comprising the general molecular formula of $A_xM_2(XO_4)_3$, where A = Na or Li; M = Ti, V, Fe and X = P, S, Mo, W, As [1–5]. In the crystal structure of NASICON framework materials, the MO_6 octahedral units share all their corners with XO_4 tetrahedra. However, the XO_4 tetrahedral units share all three corners with MO_6 octahedra. This enables the generation of interstitial and conduction channels along the *c*-axis direction, in which alkali metal ions (Na^+ or Li^+) can occupy the interstitial position. Further, the arrangement of such MO_6 octahedral units enables inferior electronic-conducting profiles, which nevertheless provide flat charge–discharge curves that are mainly ascribed to the inductive effect of polyanion groups present in it. Based on the choice of transition metal ion and its oxidation state, the NASICON-type materials are classified into anodic and cathodic applications for LIBs. For example, $LiTi_2(PO_4)_3$ and $NaTi_2(PO_4)_3$ are prospective 2.6 V vs. Li-insertion anode materials for LIBs [4]. The phosphate polyanion framework $Li_3Fe_2(PO_4)_3$ has been considered as ~2.8 V vs. Li anode material for LIBs. The redox potential has

been substantially varied not only because of transition metal cations, but also because of the polyanionic group. In $Li_3Fe_2(XO_4)_3$, where X = As, P, Mo, and S, the $Fe^{2+/3+}$ redox couple showed a reduction potential of ~2.6, ~2.9, ~3, and ~3.6 V vs. Li for $Li_3Fe_2(AsO_4)_3$, $Li_3Fe_2(PO_4)_3$, $Li_3Fe_2(MoO_4)_3$, and $Li_3Fe_2(SO_4)_3$ phases, respectively [1, 6, 7].

As a NASICON-type compound, $Li_3V_2(PO_4)_3$ is getting much more attention than other polyanion framework materials because of the multiple oxidation states of transition metal vanadium [1, 3]. $Li_3V_2(PO_4)_3$ can be used as both anode and cathode for LIBs, for example, the reduction of V^{3+} to V^{2+} can be effectively utilized as ~1.7 V vs. Li-insertion anode material by two-phase reaction with a theoretical capacity of 132 mAh g^{-1} [8]. At the same time, the $V^{3+/4+}$ redox couple can be exploited around ~4 V vs. Li by two-phase reaction and subsequent partial oxidation of V^{4+} to V^{5+} at ~4.6 V vs. Li with a theoretical capacity of 197 mAh g^{-1} for complete removal of 3 mol of lithium. However, extracting the 3 mol of lithium is too complicated in conventional solutions, since the thermodynamic stability of the electrolyte solution is up to 4.6 V vs. Li only [9]. Moreover, during discharge, it forms a solid-solution instead of two-phase reaction for insertion of 2 mol of lithium, and this leads to a severe structural change that induces capacity fading during cycling. Further, the intrinsic conductivity and vanadium dissolution are other barriers for attaining the theoretical capacity of the $Li_3V_2(PO_4)_3$ cathodes. Hence, an attempt has been made to synthesize and optimize the $Li_3V_2(PO_4)_3$ by conventional solid-state approach.

In-situ carbon coating has also been adopted to improve the electronic-conducting properties of the $Li_3V_2(PO_4)_3$ phase by using adipic acid (AA). The presence of a carbon layer is expected to prevent the direct reactivity with the electrolyte solution and thereby improve cell performance. The following precursors have been utilized in the fabrication of in-situ carbon coating to improve the electrochemical performance of monoclinic $Li_3V_2(PO_4)_3$: glucose [10–13], starch [11], polyvinylidenefluoride (PVDF) [11], stearic acid [14], polystyrene [15], citric acid [11, 16, 17], sucrose [18], maltose [19] humic acid [18], oxalic acid [13, 19], polyethylene glycol [20], and phenolic resin [21]. Moreover, V-site dopings such as Ti^{4+}, Zr^{4+}, Fe^{3+}, Al^{3+}, Cr^{3+}, Sc^{3+}, Y^{3+}, Ce^{3+}, Mg^{2+}, Mn^{2+} , and Co^{2+} were also carried out along with carbon coating to improve the electrochemical performance by stabilizing the structure during high-voltage cycling [22–24].

On the basis of this research background, AA was chosen as source material for carbon, and its concentration was varied according to the total metal ion composition present in the $Li_3V_2(PO_4)_3$ compound. The effective role of AA in the synthesis of other polyanion framework materials has already been described in our previous articles [25–34]. Comprehensive electrochemical studies were carried out for $Li_3V_2(PO_4)_3$, and the experimental results are described in detail.

2 Experimental

A conventional solid-state approach was adopted to synthesize the $Li_3V_2(PO_4)_3$ by tuning three experimental parameters: precalcination temperature, final sintering temperature, and carbon coating. High-purity Li_2CO_3 (Wako, Japan), V_2O_5 (Sigma-Aldrich, USA), $(NH_4)_2HPO_4$ (Sigma-Aldrich, USA) and AA (Sigma-Aldrich, USA) were used as starting materials. Stoichiometric amounts of Li_2CO_3, V_2O_5 , and $(NH_4)_2HPO_4$ were finely ground in an agate mortar and calcined at two different temperatures, i.e., 300 and 400 °C, for 4 h in air atmosphere using a box furnace for the decomposition of hydroxyl and ammonium moieties. The intermediate was ground again to form a pellet and fired at from 800 to 950 °C for 8 h under Ar flow to yield phase-pure $Li_3V_2(PO_4)_3$. The same procedure was repeated for synthesizing carbon-coated $Li_3V_2(PO_4)_3$ by varying the AA concentration.

Thermal studies were conducted using thermogravimetric–differential thermal analysis (TG–DTA) using a thermal analyzer system (STA 1640, Stanton Redcroft Inc., UK) with a thin Pt plate as the sample holder. The powder was heated at 5 °C min^{-1} and cooled at 10 °C min^{-1}. The structural properties of the synthesized $Li_3V_2(PO_4)_3$ phases were analyzed by using powder X-ray diffraction (XRD, Rint 1000, Rigaku, Japan) equipped with CuKα radiation. The morphological features of the powders were analyzed by field emission–scanning electron microscopy (FE–SEM, S4700, Hitachi, Japan) and transmission electron microscopy (TEM, TECNAI, Philips, Netherlands). The particle size distribution was analyzed using a dynamic light scattering (DLS) system (DLS-7000(AL), Otsuka Electronics, Japan). The CR 2032 coin-cell was used to study the electrochemical properties of $Li_3V_2(PO_4)_3$ in two-electrode assembly. The test electrodes were prepared by weighing an accurate amount of active material ($Li_3V_2(PO_4)_3$, 20 mg), 3 mg of Ketzen black, and 3 mg of conductive binder (Teflonized acetylene black, TAB-2). The composite was formulated and pressed up on a 200 mm^2 stainless steel mesh, which served as the current collector. The electrodes were dried at 160 °C for 4 h in a vacuum oven before conducting cell assembly under Ar-filled glove box. The test cells were constructed with a composite cathode and metallic lithium anode, separated by a porous polypropylene film (Celgard 3401, USA). The electrolyte solution consisting of 1 M $LiPF_6$ in ethylene carbonate : dimethyl carbonate (1:1 by vol.) was obtained from Techno

Semichem Co., Ltd., Korea. Cyclic voltammetry (CV), and electrochemical impedance spectroscopy (EIS) studies were conducted by two-electrode setup using a Bio-Logic electrochemical work station (SP-150, Biologic, France), in which metallic lithium acts as both working and counter electrodes. Galvanostatic cycling studies were carried out between 3 and 4.8 V vs. Li with different current densities in ambient temperature conditions.

3 Results and discussion

Figure 1 presents the TG–DTA traces of the precursor used for synthesizing a $Li_3V_2(PO_4)_3$ phase under Ar environment. The TGA curve can be broadly divided into three regions: ~40–200, 200–600 °C, and beyond 600 °C. The first region shows minimum weight loss (~2 %) and mainly corresponds to the removal of moisture during sample loading. However, the second region exhibited a weight loss of about 26 % that was attributed to the decomposition of Li_2CO_3 ($Li_2CO_3 \rightarrow Li_2O + CO_2$) and ammonium moieties. Apart from the decomposition of the starting materials, nucleation growth takes place to form $Li_3V_2(PO_4)_3$ phase. The third region in both TGA and DTA clearly reveals the absence of any weight loss until 1,000 °C. This TG–DTA study demonstrates that the NASICON-type monoclinic $Li_3V_2(PO_4)_3$ phase could be prepared beyond 600 °C under an inert atmosphere by solid-state approach.

From the broader decomposition region between 200 and 600 °C clearly shown in the TG–DTA curve, we attempted to study the effect of precalcination temperature during the synthesis of $Li_3V_2(PO_4)_3$. The $Li_3V_2(PO_4)_3$ phase was pre-calcined at two different temperatures, namely 300 and 400 °C, for 4 h and subsequently sintered for various temperatures from 800 to 950 °C for 8 h. The precalcination was carried out under normal air atmosphere and the final heat treatment was conducted under Ar flow. Figure 2 shows the XRD pattern of the $Li_3V_2(PO_4)_3$ phase synthesized at 300 °C for 4 h with subsequent final calcinations. In the XRD pattern, the material prepared at 800 and 850 °C does not exhibit any characteristic peaks, which is indicative of incomplete $Li_3V_2(PO_4)_3$ formation. At 900 °C, the XRD pattern clearly shows the formation of phase-pure $Li_3V_2(PO_4)_3$ without any impurity traces. However, the XRD patterns clearly showed the suppression of the $Li_3V_2(PO_4)_3$ phase when the temperature exceeds 900 °C (minor intensity peaks around ~ 14 and 16° and reduction in the intensity of the rest of the reflections). This indicates the influence of nucleation growth, which occurred at precalcination temperature. Figure 3 illustrates the XRD patterns of $Li_3V_2(PO_4)_3$ pre-calcined at 400 °C for 4 h and subsequently sintered at high temperatures from 850 to 950 °C. Similar to the above case, the phase formation is not completed at 850 °C and impurities such as Li_3PO_4 and $LiVP_2O_7$ are evident. In contrast to the precalcination at 300 °C for 4 h, 900 and 950 °C sintered powders show the characteristic reflections with increase in characteristic peak intensities, which confirms the formation of $Li_3V_2(PO_4)_3$ phase. Moreover, variation in intensities of the XRD reflections at final calcination temperature provides the influence of precalcination temperature (300 and 400 °C) during the formation of single-phase $Li_3V_2(PO_4)_3$ powders.

The morphologic features of the $Li_3V_2(PO_4)_3$ phases synthesized in the above conditions are presented in Fig. 4. The powders prepared at 900 °C clearly show a particulate morphology, irrespective of the precalcination temperature

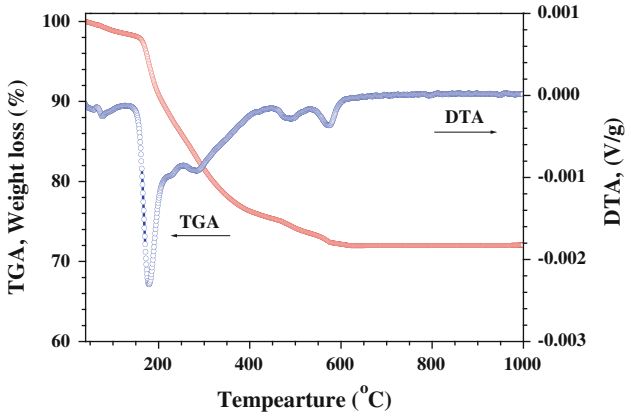

Fig. 1 Thermogravimetric–differential thermal analysis (TG–DTA) traces of the precursors used to synthesize the $Li_3V_2(PO_4)_3$ under Ar atmosphere

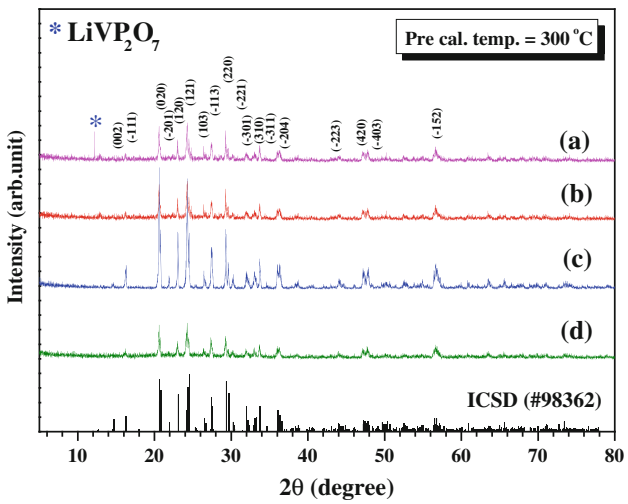

Fig. 2 X-ray diffraction patterns of $Li_3V_2(PO_4)_3$ materials obtained at different temperatures by solid-state method. Pre-calcined samples at 300 °C for 4 h are re-calcined at (*a*) 800 °C, (*b*) 850 °C, (*c*) 900 °C and (*d*) 950 °C for 8 h

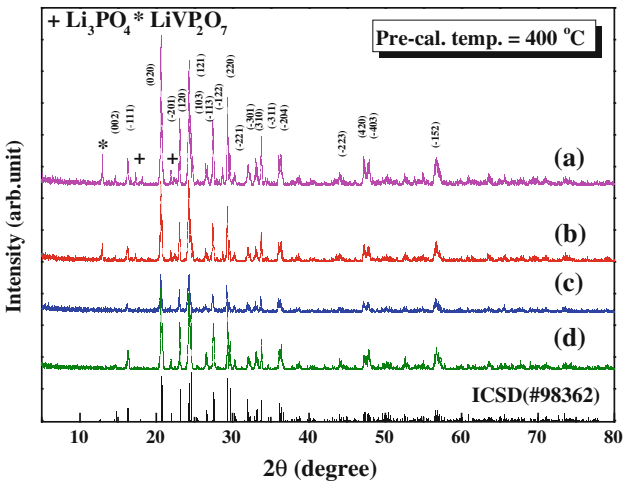

Fig. 3 X-ray diffraction patterns of $Li_3V_2(PO_4)_3$ materials obtained at different temperatures by solid-state method. Pre-calcined samples at 400 °C for 4 h are re-calcined at (*a*) 800 °C, (*b*) 850 °C, (*c*) 900 °C and (*d*) 950 °C for 8 h

(Fig. 4a, c). When the sintering temperature is increased to 950 °C, highly aggregated particulate morphology is evident in Fig. 4b, d. Only this kind of aggregation was expected because the material was sintered at high temperature with a relatively longer duration of 8 h. In general, particulate morphology is preferential for the formulation of good electrodes. Hence, better electrochemical properties are expected for the samples sintered at 900 °C in both cases. In order to establish an appropriate synthesis condition to yield high-performance $Li_3V_2(PO_4)_3$ material, test electrodes were formulated, and studies were conducted in half-cell configurations ($Li/Li_3V_2(PO_4)_3$).

In this study, the influence of electrochemical performance of the $Li_3V_2(PO_4)_3$ phase materials synthesized at various precalcination and sintering temperatures was tested between 3 and 4.8 V vs. Li at a current density of 0.1 mA cm^{-2} at room temperature. The galvanostatic charge–discharge curves of $Li/Li_3V_2(PO_4)_3$ are given in Fig. 5. The cell displayed initial discharge capacities of 158 and 156 mAh g^{-1} for the material pre-calcined at 300 °C and subsequently fired at 900 and 950 °C, respectively, compared to 156 and 151 mAh g^{-1}, for that pre-calcined at 400 °C and sintered at 900 and 950 °C, respectively. The maximum theoretical capacity of the phases was limited to ~ 77–80 %. A detailed description of this kind of behavior is presented below. Moreover, the differences in the initial discharge capacities between the four samples were negligible, and it is too difficult to predict the best-performing material at this point. Hence, the cycling studies were extended for a few more cycles to locate the appropriate synthesis conditions for attaining high-performance NASICON-type $Li_3V_2(PO_4)_3$, and the cycling performances of those half-cells are presented in Fig. 6. All four $Li_3V_2(PO_4)_3$ phases clearly experienced capacity fade during cycling. On the other hand, $Li_3V_2(PO_4)_3$ prepared at 300 °C pre-calcined and subsequently heat treated at 900 °C showed better cycling profiles than those under the other synthesis conditions. As a consequence, a precalcination temperature of 300 °C for 4 h and a sintering temperature of 900 °C for 8 h were chosen for further studies to optimize the use of carbon-coated $Li_3V_2(PO_4)_3$ particulates with AA as a carbon source.

Figure 7 displays the XRD patterns of the $Li_3V_2(PO_4)_3$ powders with various concentrations of AA (0, 0.05, 0.1, and 0.15 M) relative to the total metal ion composition in the phase. All the prepared phases exhibited well-defined reflections, which is indicative of the highly crystalline nature of the materials synthesized. No impurity phases were noted in the observed patterns after the inclusion of different molar concentrations of AA for carbon coating. This suggested that the amount of carbon precursor/carbon was too small to induce the formation of impurities like V_2O_3. The observed satellite peaks were indexed according to the monoclinic structure with a $P2_1/n$ space group and were consistent with the literature (JCPDS No.: 80-1515). As described earlier, $Li_3V_2(PO_4)_3$ is composed of a three-dimensional arrangement of VO_6 octahedra and PO_4 tetrahedra sharing oxygen vertices. Each VO_6 octahedral unit is surrounded by six PO_4 tetrahedral units and, similarly, each tetrahedral unit is surrounded by four VO_6 octahedral units. This kind of linkage forms a three-dimensional network, and the alkali cation, Li, is located in the cavities within the framework. Three fourfold crystallographic positions exist for the lithium atoms, leading to 12 lithium positions within the unit-cell. Further, the strong covalent bond between P–O necessitated thermal stability for NASICON-type $Li_3V_2(PO_4)_3$ materials in both the lithiated and de-lithiated phases. Hence, the monoclinic $Li_3V_2(PO_4)_3$ phase is expected to exhibit an improved electrochemical performance after the carbonization of AA.

DLS experiments were conducted to study the influence of AA concentration during the synthesis of $Li_3V_2(PO_4)_3$ phase. The same number of $Li_3V_2(PO_4)_3$ phase materials was dispersed in absolute ethanol and sonicated before the experiment was conducted. Figure 8 presents the DLS results of $Li_3V_2(PO_4)_3$ phases with different molar concentrations of (0, 0.05, 0.1, and 0.15 M against total metal ion composition in the compound) AA, pre-calcined and calcined at 300 and 900 °C. As expected, there is no obvious difference between the particles sizes among all the AA concentrations. However, the higher AA concentration (0.15 M) showed the dominant particle size distribution with a range of ~ 150–200 nm. The AA concentration used in the present study was too small to suppress the particle

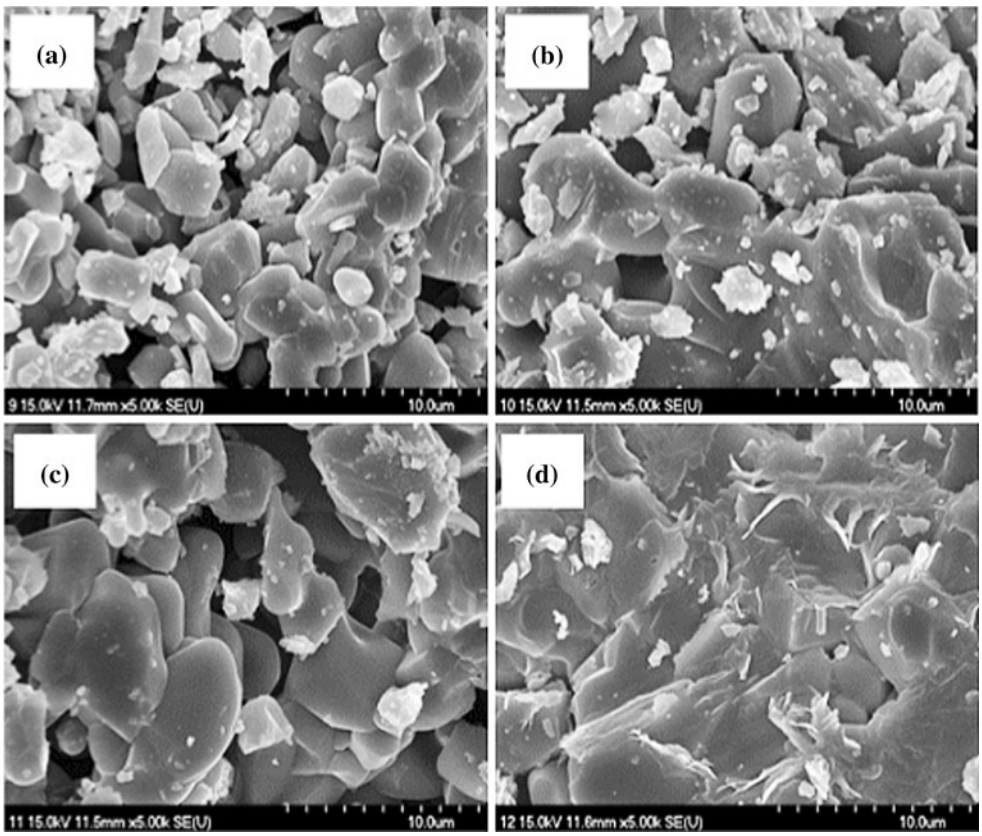

Fig. 4 Scanning electron microscopic (SEM) images of $Li_3V_2(PO_4)_3$ materials. The samples pre-calcined at 300 °C for 4 h are re-calcined at **a** 900 °C and **b** 950 °C for 8 h. The samples pre-calcined at 400 °C for 4 h are re-calcined at **c** 900 °C and **d** 950 °C for 8 h

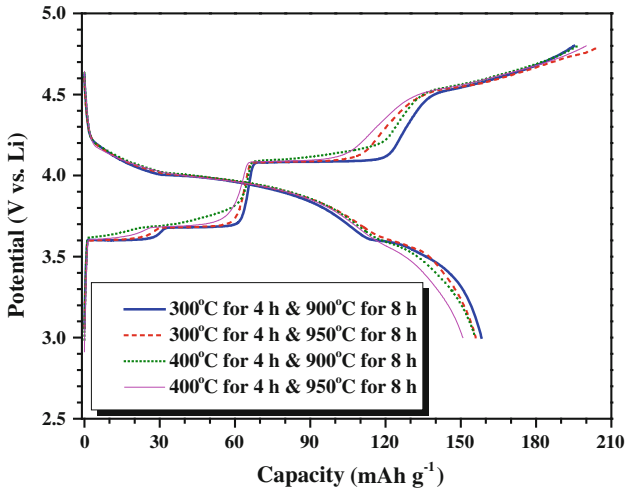

Fig. 5 Initial charge–discharge curves of $Li/Li_3V_2(PO_4)_3$ cells cycled between 3–4.8 V vs. Li at the current density of 0.1 mA cm^{-2}

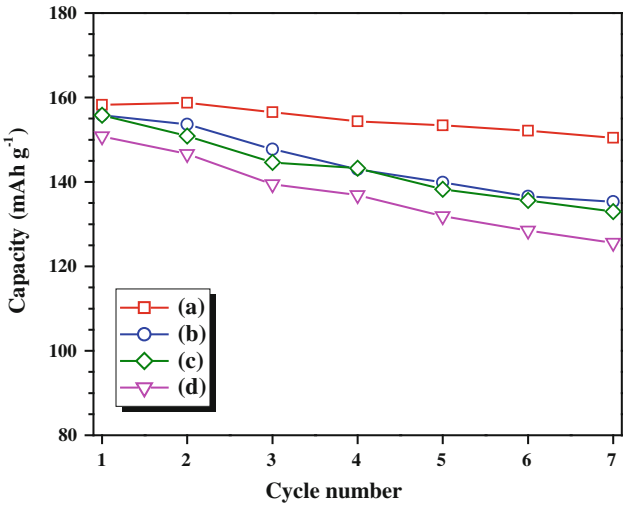

Fig. 6 Cycleability of $Li/Li_3V_2(PO_4)_3$ cells. Samples pre-calcined at 300 °C for 4 h are re-calcined at (*a*) 900 °C and (*b*) 950 °C for 8 h. Samples pre-calcined at 400 °C for 4 h are re-calcined at (*c*) 900 °C and (*d*) 950 °C for 8 h

growth. In addition to the AA concentration, the high final calcination temperature of 900 °C for the longer duration of 8 h cannot be ruled out as the cause of the growth of such particles.

To analyze the surface features of the $Li_3V_2(PO_4)_3$ phases, SEM images were recorded and are presented in Fig. 9. In the absence of any obvious differences in the particle sizes in the DLS analysis results, only pristine $Li_3V_2(PO_4)_3$ powder with the maximum AA concentration of 0.15 M was subjected to SEM analysis. The pristine

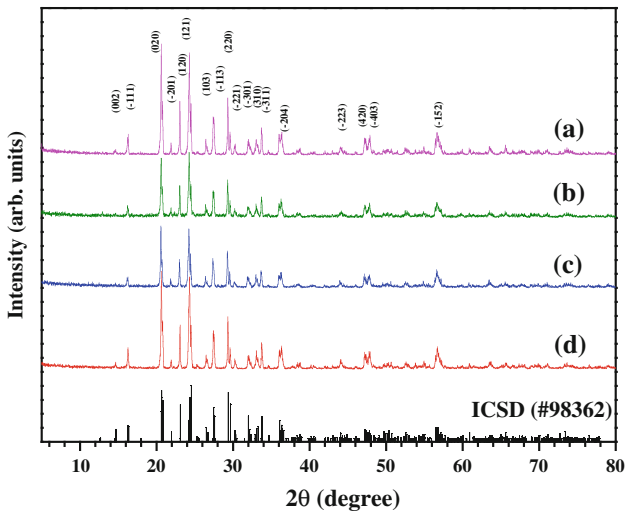

Fig. 7 X-ray diffraction patterns of C-$Li_3V_2(PO_4)_3$ materials obtained by solid-state method. The molar ratios of adipic acid to total metal ions are (*a*) 0, (*b*) 0.05, (*c*) 0.1 and (*d*) 0.15

$Li_3V_2(PO_4)_3$ powders exhibited a smooth particulate morphology, whereas the carbon-coated $Li_3V_2(PO_4)_3$ (0.15 M AA) showed weak aggregation with rough morphology. To ensure that the carbon layer over the $Li_3V_2(PO_4)_3$ particles was retained during the carbonization of AA in the synthesis procedure, a high-resolution TEM (HR-TEM) was conducted. The resulting HR-TEM micrograph (Fig. 9c) clearly reveals a thin layer of carbon (~3 nm) on the surface of the particles, which we believe improves the conducting profiles of the $Li_3V_2(PO_4)_3$ phase and thereby facilitates the extraction of more lithium with minimum of capacity fade.

The electrochemical performances of pristine and carbon-coated $Li_3V_2(PO_4)_3$ were evaluated in half-cell configurations between 3 and 4.8 V vs. Li at current density of 0.1 mA cm^{-2} at room temperature. Galvanostatic charge–discharge curves of the half-cell results are presented in Fig. 10. The test cells displayed initial discharge capacities of 153, 151, 159, and 178 mAh g^{-1} for 0, 0.05, 0.1 and 0.15 M concentrations of AA, respectively, to the total metal ion composition in the $Li_3V_2(PO_4)_3$ phase. In all the four cases, the first charge capacity exceeds the theoretical capacity (197 mAh g^{-1}) of $Li_3V_2(PO_4)_3$ for the removal of 3 mol of lithium, which was mainly attributed to the decomposition of the electrolyte solution, apart from the complete removal of three lithium ions to form the $V_2^{4+/5+}(PO_4)_3$ phase. The thermodynamic conventional carbonate-based solutions are stable only up to ~ 4.6 V (vs. Li) [9]. Pristine and carbon-coated (0.05 AA) $Li_3V_2(PO_4)_3$ showed almost the same first discharge capacity (~ 2.3 mol of lithium), which indicates an insufficient carbon presence (i.e., AA concentration) to improve the conducting profiles and subsequently extract 3 mol of lithium. When the concentration was increased to 0.1 M, slightly more lithium (~ 2.4 mol) could be extracted from the lattice. This improvement was mainly attributed to the improved electronic conductivity of NASICON-type $Li_3V_2(PO_4)_3$. A further increase in AA concentration to 0.15 M improved the lithium extraction to ~ 2.7 mol per formula unit. For this concentration, ~ 0.38 wt% carbon content is estimated by

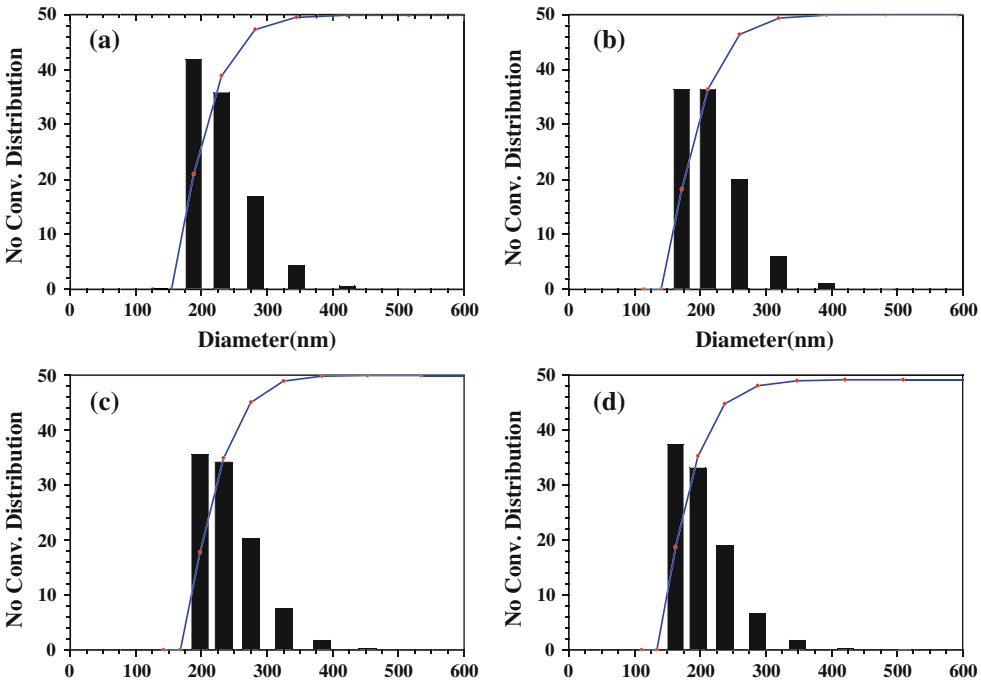

Fig. 8 Particle size distribution of C–$Li_3V_2(PO_4)_3$ obtained by various molar ratios of adipic acid to total metal ions **a** 0, **b** 0.05, **c** 0.1 and **d** 0.15

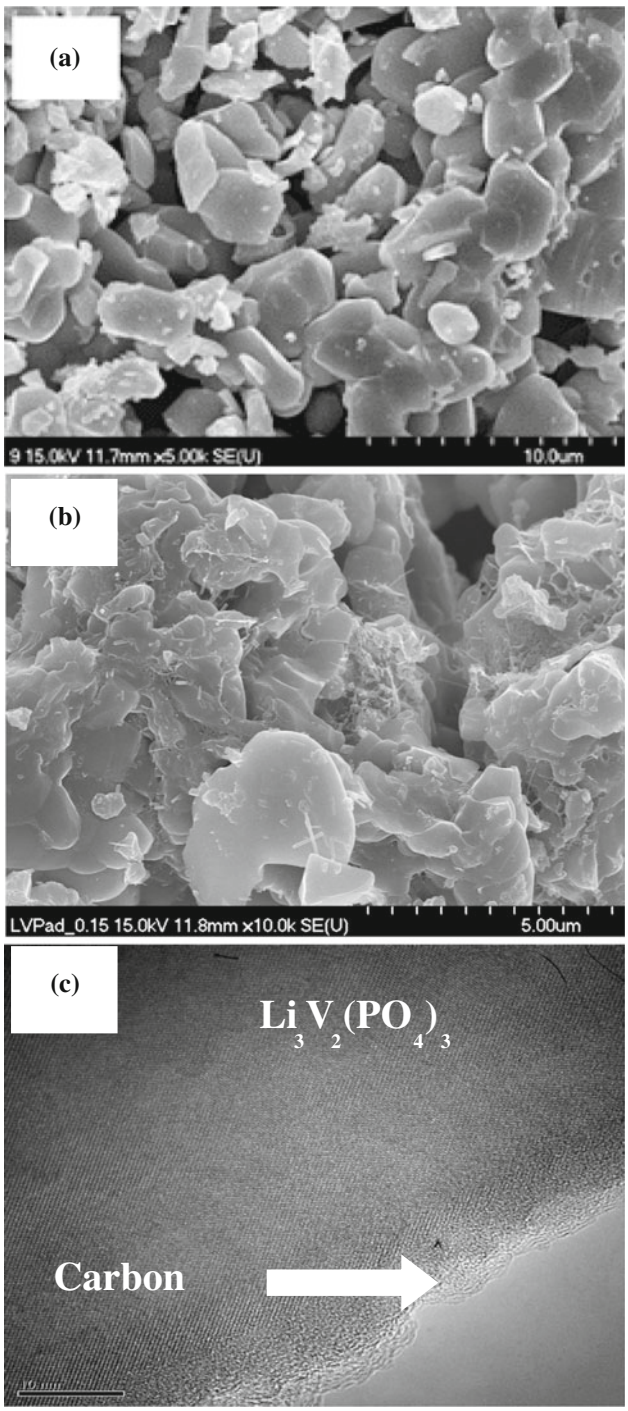

Fig. 9 Scanning electron microscopic (SEM) images of **a** pristine and **b** carbon-coated $Li_3V_2(PO_4)_3$ materials (molar ratio of adipic acid to total metal ions are 0.15). **c** High-resolution transmission electron microscopic (HR-TEM) picture of carbon-coated $Li_3V_2(PO_4)_3$

elemental analysis. However, we did not attempt to increase the AA concentration beyond 0.15 M, since an excessive presence of organic precursor has a detrimental effect on the electrode materials prospect.

We have previously reported that an increase in the AA concentration raises the carbon content in the resultant

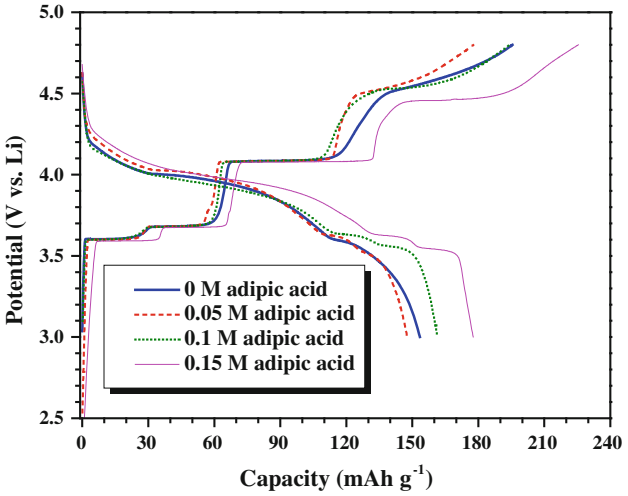

Fig. 10 Initial charge–discharge curves of Li/C-$Li_3V_2(PO_4)_3$ cells cycled between 3–4.8 V vs. Li at 0.1 mA cm^{-2} with various concentrations of adipic acid to total metal ions ratios

$Li_3V_2(PO_4)_3$ phase, which in turn dilutes the presence of active materials and hence reduces the volumetric capacity [32]. Moreover, high-temperature synthesis for a prolonged time leads to possible carbothermal reduction reactions and subsequent formation of impurity phases along with the native phase. Irrespective of carbon coating, all the $Li_3V_2(PO_4)_3$ phases undergo multiple Li-extraction/insertion steps during electrochemical cycling. In the charging process, the removal of 1 mol lithium occurs according to the two-phase reaction in two steps: ~ 3.6 V vs. Li ($Li_{2.5}V_2^{3+/4+}(PO_4)_3$), and ~ 3.7 V vs. Li ($Li_2V_2^{3+/4+}(PO_4)_3$). The second lithium is removed at ~ 4.1 V vs. Li to form $Li_1V_2^{4+}(PO_4)_3$, which preserves the monoclinic symmetry of the lattice [35]. Further, a well-defined and long plateau has been observed at ~ 4.1 V vs. Li, which is indicative of a bi-phase reaction and corresponds to the $V^{3+/4+}$ redox couple. The final lithium is extracted at ~ 4.55 V vs. Li to form a de-lithiated ($Li_0V_2(PO_4)_3$) phase, in which V is in a mixed valance state of V^{4+} and V^{5+}. Conversely, during the discharge process, the $Li_3V_2(PO_4)_3$ phase exhibits unusually than Li-extraction (In the charging process, Li-ions are extracted by a two-phase reaction, whereas during discharge, Li-ions are inserted by single-phase reaction). A monotonous discharge curve is observed for the re-insertion of the first two lithium ions ($Li_0V_2(PO_4)_3 \rightarrow Li_2V_2(PO_4)_3$), which clearly reveals the formation of solid-solution behavior [35, 36]. However, the re-insertion of the other lithium induces a two-phase reaction in a two-step process at ~ 3.55 V vs. Li ($Li_2V_2(PO_4)_3 \rightarrow Li_{2.5}V_2(PO_4)_3$) and ~ 3.6 V vs. Li ($Li_{2.5}V_2(PO_4)_3 \rightarrow Li_3V_2(PO_4)_3$). In most cases, the researchers are not interested in extracting the third lithium ion to retain the two-phase reaction mechanism (the upper cut-off potential was restricted to 4.3 V vs. Li) in charging processes

involving compromised discharge capacity. The challenging task with $Li_3V_2(PO_4)_3$ is to extract the third lithium ion and subsequently improve the cell cycleability.

The cycling profiles of pristine and carbon-coated $Li_3V_2(PO_4)_3$ powders in half-cell configurations up to 50 cycles are illustrated in Fig. 11. All the $Li_3V_2(PO_4)_3$ phase materials experienced capacity fade during cycling. Among the various AA concentrations, the $Li_3V_2(PO_4)_3$ phase comprising 0.15 M exhibited a better cycling profile. After 50 cycles, the cells displayed discharge capacities of 110, 103, 116, and 147 mAh g^{-1} for 0, 0.05, 0.1, and 0.15 M AA concentrations, respectively. Capacity retention of 72, 68, 73, and 83 % of the initial discharge capacity was maintained after 50 cycles for 0, 0.05, 0.1, and 0.15 M AA concentrations, respectively. The observed capacity retentions are superior to those of other source materials such as citric acid, glucose, PVDF, and starch, the cells of which exhibited discharge capacities of 144, 135, 130, and 131 mAh g^{-1} after 50 cycles, respectively [11], compared to $\sim$ 148 mAh g^{-1} for the carbon-coated $Li_3V_2(PO_4)_3$ (0.15 M AA) after 50 cycles. Similarly, cells with double carbon sources such as oxalic acid and glucose displayed a capacity retention of 139 mAh g^{-1} after 50 cycles [13]. The improved performance of the $Li_3V_2(PO_4)_3$ phases examined in this study was mainly attributed to the appropriate synthesis conditions and, more importantly, the use of AA as a carbon precursor. We have previously investigated the implications of AA as a source material for other polyanion hosts such as $LiFePO_4$ [28–30], Li_2FeSiO_4 [27], Li_2MnSiO_4 [26, 31–34], and $LiMnBO_3$ [25] and found excellent improvements in the electrochemical performance. Although capacity fading has been attributed to several reasons in addition to electrolyte decomposition, vanadium dissolution in the electrolyte solution during high-voltage charging is the prime factor [37]. At higher concentrations, the presence of a carbon layer certainly prevents a direct reaction with the electrolyte and provides better cell cycleability.

To evaluate the influence of carbon under high currents, a duplicate cell was fabricated to study the rate performance at room temperature for configuration between 3 and 4.8 V vs. Li. The rate performances of carbon-coated (0.15 M AA) and pristine $Li_3V_2(PO_4)_3$ are presented in Fig. 12. The carbon-coated $Li_3V_2(PO_4)_3$ cell showed discharge capacities of 173, 165, 150, 132, 105, and 76 mAh g^{-1} at rates of 0.1, 0.2, 0.5, 1, 5, and 12 C, respectively, compared to only 155, 148, 141, 87, 51, and 31 mAh g^{-1}, respectively, for the pristine material under the same testing conditions. The discharge capacity decreased with increasing current rate, which was attributed to the reduced participation of the active material, i.e., only the surface of the active material participated in the reaction [38]. The improved performance of the carbon-

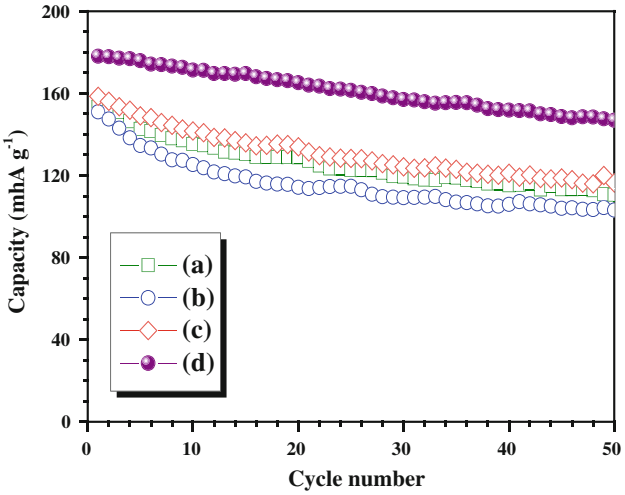

Fig. 11 Cycling profiles of Li/C-$Li_3V_2(PO_4)_3$ cells cycled between 3-4.8 V vs. Li at 0.1 mA cm^{-2} with various concentrations of adipic acid to total metal ions ratios (*a*) 0, (*b*) 0.05 M, (*c*) 0.1 M and (*d*) 0.15 M

coated $Li_3V_2(PO_4)_3$ compared with the pristine phase was expected due to the role of the carbon layer over the particulates in providing the necessary conducting pathways for faster electron transport under such high current rates.

CV is an excellent tool to investigate electrochemical reactions, particularly in electrode materials for LIBs. The CV traces of Li/carbon-coated (0.15 M AA) and pristine $Li_3V_2(PO_4)_3$ were recorded between 3 and 4.8 V vs. Li at a scan rate of 0.1 mV s^{-1}, and the results are presented in Fig. 13. The CV signatures were recorded in standard two-electrode configuration, in which metallic lithium acts as both the counter and reference electrode. The test cell showed an open circuit potential of $\sim$ 3 V vs. Li for both

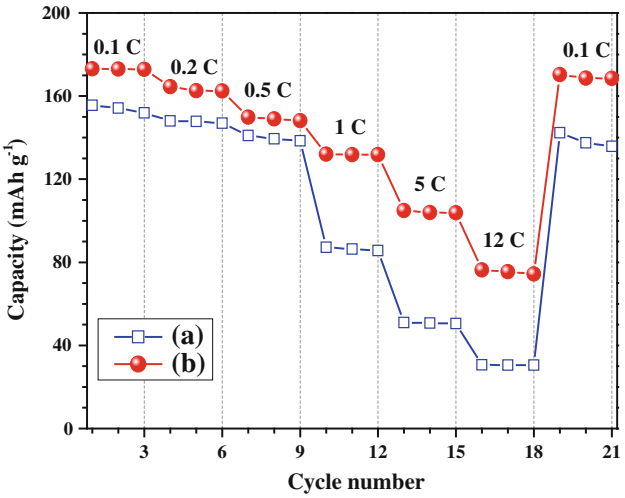

Fig. 12 Rate performances of (*a*) pristine and (*b*) carbon-coated-$Li_3V_2(PO_4)_3$ (adipic acid to total metal ion ratio is 0.15) half-cells cycled between 3–4.8 V vs. Li in room temperature

carbon-coated and pristine $Li_3V_2(PO_4)_3$ powders, and the test cell was first charged to extract the Li-ions. In the anodic sweep, the cell showed two well-defined and sharp oxidation potentials of ~ 3.65 and ~ 3.73 V vs. Li, which corresponded to the removal of 1 mol lithium (oxidation of 1 mol V^{3+} into V^{4+}). At ~4.14 V vs. Li, the test cell showed another sharp oxidation peak corresponding to the removal of 1 mol of lithium ions (complete oxidation of V^{3+} into V^{4+}). However, the broad oxidation potential at ~ 4.48 V vs. Li correlates to the removal of the third lithium ion from the $Li_3V_2(PO_4)_3$ lattice to form the $Li_0V_2(PO_4)_3$ phase. The well-defined sharp oxidation potential evident during the anodic scan is ascribed to the two-phase reaction mechanism, whereas the broader peak potential corresponds to the solid-solution behavior. In the cathodic scan, the reduction potential at ~ 3.94 V vs. Li with a broader peak indicates the insertion of 2 mol of lithium with solid-solution behavior. The sharp peak potentials at ~3.58 and 3.49 V vs. Li are ascribed to the insertion of 1 mol of lithium by two-step process according to the bi-phase mechanism. An obvious difference in the Li-kinetic properties is also clearly apparent: the carbon-coated $Li_3V_2(PO_4)_3$ phase shows well-defined peaks during both anodic and cathodic scans, whereas pristine $Li_3V_2(PO_4)_3$ shows sluggish behavior. These improved Li-kinetic properties of carbon-coated $Li_3V_2(PO_4)_3$ are due to the better electronic conducting-properties of the electrode, which allows the faster transportation of electrons, thereby enabling facile diffusion of Li-ions. The observed CV traces are consistent with the galvanostatic charge–discharge profiles and complement the reaction mechanism described above.

To establish the effect of AA concentration/carbon content on the electronic-conducting profiles, EIS was conducted, and the results are presented in Fig. 14. EIS spectroscopy was conducted in a two-electrode coin-cell configuration. All the $Li_3V_2(PO_4)_3$ powders showed a semicircle followed by a vertical tail inclined at 45°. In general, the appearance of a high-frequency semicircle is attributed to the formation of a solid electrolyte interface film and/or contact resistance, the medium-frequency region is assigned to the charge-transfer impedance across the electrode/electrolyte interface, and a vertical tail at a line inclined 45° to the real axis corresponds to the lithium diffusion kinetics known as the Warburg tail [39]. The diameter of the semicircles in the medium-frequency region is decreased with the increasing AA concentration, indicating that increasing the AA concentration (or carbon content) drastically enhances the electronic-conducting profiles by reducing the charge-transfer resistance. This improvement in electronic-conductivity profile was well reflected in the electrochemical Li-insertion/extraction, rate performance studies, and CV measurements, when

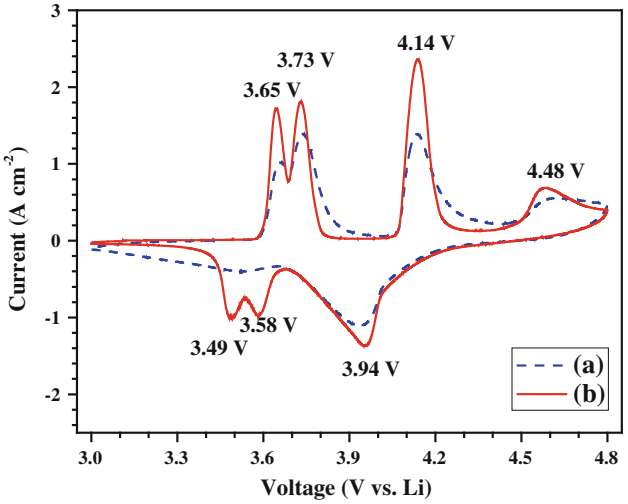

Fig. 13 Cyclic voltammetric (CV) traces of (*a*) pristine and (*b*) carbon-coated-$Li_3V_2(PO_4)_3$ (adipic acid to total metal ion ratio is 0.15) cycled between 3-4.8 V vs. Li at scan rate of 0.1 mV s^{-1}, in which metallic lithium serves as a counter and reference electrode

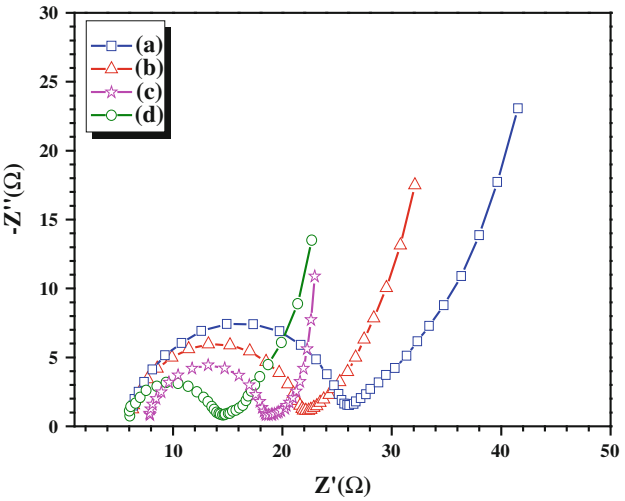

Fig. 14 Electrochemical impedance spectroscopic (EIS) curves of $Li_3V_2(PO_4)_3$ phase with various concentrations of adipic acid to total metal ions (*a*) 0, (*b*) 0.05, (*c*) 0.1 and (*d*) 0.15

compared to pristine $Li_3V_2(PO_4)_3$ phase. The EIS study clearly verified the improvement of conducting profiles with the increasing AA concentration.

4 Conclusion

High-performance carbon-coated $Li_3V_2(PO_4)_3$ was prepared by conventional solid-state approach under the optimized conditions of precalcination at 300 °C for 4 h and sintering at 900 °C for 8 h in an Ar atmosphere. AA was used as the source material for carbon, and its

concentration was varied according to the total metal ion composition in the NASICON-type $Li_3V_2(PO_4)_3$. The obtained phases were characterized by XRD, SEM, TEM, and particle size distributions. The electrochemical properties were evaluated in half-cell configurations between 3 and 4.8 V vs. Li at the current density of 0.1 mA cm^{-2}. A half-cell with Li/carbon-coated $Li_3V_2(PO_4)_3$ (0.15 M AA) delivered discharge capacities of 178 and 143 mAh g^{-1} for the 1st and 60th cycles, respectively. The carbon presence improved the cycling profiles, which exhibited a capacity retention of 80 % after 60 cycles. CV and EIS were also conducted to validate the reaction mechanism and conductivity profiles, respectively. To summarize, the results of the present study results clearly demonstrated that AA can be effectively used to improve the electrochemical performance of the NASICON-type $Li_3V_2(PO_4)_3$ for the removal of 3 mol of lithium.

Acknowledgments This study was supported by the Energy Resource R&D program under the Ministry of Knowledge Economy, Republic of Korea.

References

1. Goodenough JB, Kim Y (2009) Challenges for rechargeable Li batteries. Chem Mater 22(3):587–603. doi:10.1021/cm901452z
2. Song MK, Park S, Alamgir FM, Cho J, Liu M (2011) Nanostructured electrodes for lithium-ion and lithium-air batteries: the latest developments, challenges, and perspectives. Mater Sci Eng R 72(11):203–252. doi:10.1016/j.mser.2011.06.001
3. Gong Z, Yang Y (2011) Recent advances in the research of polyanion-type cathode materials for Li-ion batteries. Energy Environ Sci 4(9):3223–3242
4. Patoux S, Masquelier C (2002) Lithium insertion into titanium phosphates, silicates, and sulfates. Chem Mater 14(12):5057–5068. doi:10.1021/cm0201798
5. Aravindan V, Gnanaraj J, Lee Y-S, Madhavi S (2013) LiMnPO$_4$—a next generation cathode material for lithium-ion batteries. J Mater Chem A 1(11):3518–3539
6. Manthiram A, Goodenough JB (1987) Lithium insertion into $Fe_2(MO_4)_3$ frameworks: comparison of M = W with M = Mo. J Solid State Chem 71(2):349–360
7. Manthiram A, Goodenough JB (1989) Lithium insertion into $Fe_2(SO_4)_3$ frameworks. J Power Sources 26(3–4):403–408
8. Aboulaich A, Bouchet R, Delaizir G, Seznec V, Tortet L, Morcrette M, Rozier P, Tarascon JM, Viallet V, Dollé M (2011) A new approach to develop safe all-inorganic monolithic Li-ion batteries. Adv Energy Mater 1(2):179–183. doi:10.1002/aenm.201000050
9. Aravindan V, Gnanaraj J, Madhavi S, Liu HK (2011) Lithium-ion conducting electrolyte salts for Lithium batteries. Chemistry 17(51):14326–14346. doi:10.1002/chem.201101486
10. Chang C, Xiang J, Shi X, Han X, Yuan L, Sun J (2008) Hydrothermal synthesis of carbon-coated lithium vanadium phosphate. Electrochim Acta 54(2):623–627. doi:10.1016/j.electacta.2008.07.038
11. Rui XH, Li C, Chen CH (2009) Synthesis and characterization of carbon-coated $Li_3V_2(PO_4)_3$ cathode materials with different carbon sources. Electrochim Acta 54(12):3374–3380. doi:10.1016/j.electacta.2009.01.011
12. Wang L, Zhang LC, Lieberwirth I, Xu HW, Chen C-H (2010) A $Li_3V_2(PO_4)_3$/C thin film with high rate capability as a cathode material for lithium-ion batteries. Electrochem Commun 12(1):52–55. doi:10.1016/j.elecom.2009.10.034
13. Zhang L–L, Li Y, Peng G, Wang ZH, Ma J, Zhang WX, Hu X-L, Huang Y-H (2012) High-performance $Li_3V_2(PO_4)_3$/C cathode materials prepared via a sol–gel route with double carbon sources. J Alloy Compd 513:414–419. doi:10.1016/j.jallcom.2011.10.059
14. Qiao YQ, Wang XL, Xiang JY, Zhang D, Liu WL, Tu JP (2011) Electrochemical performance of $Li_3V_2(PO_4)_3$/C cathode materials using stearic acid as a carbon source. Electrochim Acta 56(5):2269–2275. doi:10.1016/j.electacta.2010.11.073
15. Qiao YQ, Wang XL, Zhou Y, Xiang JY, Zhang D, Shi SJ, Tu JP (2010) Electrochemical performance of carbon-coated $Li_3V_2(PO_4)_3$ cathode materials derived from polystyrene-based carbon-thermal reduction synthesis. Electrochim Acta 56(1):510–516. doi:10.1016/j.electacta.2010.08.053
16. Zhu XJ, Liu YX, Geng LM, Chen LB (2008) Synthesis and performance of lithium vanadium phosphate as cathode materials for lithium-ion batteries by a sol–gel method. J Power Sources 184(2):578–582. doi:10.1016/j.jpowsour.2008.01.007
17. Chen Q, Wang J, Tang Z, He W, Shao H, Zhang J (2007) Electrochemical performance of the carbon-coated $Li_3V_2(PO_4)_3$ cathode material synthesized by a sol–gel method. Electrochim Acta 52(16):5251–5257. doi:10.1016/j.electacta.2007.02.039
18. Tang A, Wang X, Liu Z (2008) Electrochemical behavior of $Li_3V_2(PO_4)_3$/C composite cathode material for lithium-ion batteries. Mater Lett 62(10–11):1646–1648. doi:10.1016/j.matlet.2007.09.064
19. Rui XH, Ding N, Liu J, Li C, Chen CH (2010) Analysis of the chemical diffusion coefficient of lithium ions in $Li_3V_2(PO_4)_3$ cathode material. Electrochim Acta 55(7):2384–2390. doi:10.1016/j.electacta.2009.11.096
20. Wang J, Liu J, Yang G, Zhang X, Yan X, Pan X, Wang R (2009) Electrochemical performance of $Li_3V_2(PO_4)_3$/C cathode material using a novel carbon source. Electrochim Acta 54(26):6451–6454. doi:10.1016/j.electacta.2009.05.002
21. Fu P, Zhao Y, Dong Y, An X, Shen G (2006) Synthesis of $Li_3V_2(PO_4)_3$ with high performance by optimized solid-state synthesis routine. J Power Sources 162(1):651–657. doi:10.1016/j.jpowsour.2006.07.029
22. Yao J, Wei S, Zhang P, Shen C, Aguey-Zinsou K-F, Wang L (2012) Synthesis and properties of $Li_3V_{2-x}Ce_x(PO_4)_3$/C cathode materials for Li-ion batteries. J Alloy Compd 532(0):49–54. doi:10.1016/j.jallcom.2012.04.014
23. Cho AR, Son JN, Aravindan V, Kim H, Kang KS, Yoon WS, Kim WS, Lee YS (2012) Carbon supported, Al doped-$Li_3V_2(PO_4)_3$ as a high rate cathode material for lithium-ion batteries. J Mater Chem 22(14):6556–6560
24. Son JN, Kim GJ, Kim MC, Kim SH, Aravindan V, Lee YG, Lee YS (2013) Carbon-coated NASICON type $Li_3V_{2-x}M_x(PO_4)_3$ (M = Mn, Fe and Al) materials with enhanced cyclability for Li-ion batteries. J Electrochem Soc 160(1):A87–A92. doi:10.1149/2.039301jes
25. Aravindan V, Karthikeyan K, Amaresh S, Lee YS (2010) LiMnBO$_3$/C: a potential cathode material for lithium batteries. Bull Korean Chem Soc 31(6):1506–1508
26. Aravindan V, Karthikeyan K, Amaresh S, Lee YS (2011) Superior lithium storage properties of carbon-coated Li_2MnSiO_4 cathodes. Electrochem Solid-State Lett 14(4):A33–A35
27. Karthikeyan K, Aravindan V, Lee SB, Jang IC, Lim HH, Park GJ, Yoshio M, Lee YS (2010) A novel asymmetric hybrid supercapacitor based on Li_2FeSiO_4 and activated carbon electrodes. J Alloy Compd 504(1):224–227
28. Lee SB, Jang IC, Lim HH, Aravindan V, Kim HS, Lee YS (2010) Preparation and electrochemical characterization of $LiFePO_4$ nanoparticles with high rate capability by a sol–gel method. J Alloy Compd 491(1–2):668–672

29. Lim HH, Jang IC, Lee SB, Karthikeyan K, Aravindan V, Lee YS (2010) The important role of adipic acid on the synthesis of nanocrystalline lithium iron phosphate with high rate performance. J Alloy Compd 495(1):181–184
30. Son CG, Yang HM, Lee GW, Cho AR, Aravindan V, Kim HS, Kim WS, Lee YS (2011) Manipulation of adipic acid application on the electrochemical properties of $LiFePO_4$ at high rate performance. J Alloy Compd 509(4):1279–1284
31. Aravindan V, Ravi S, Kim WS, Lee SY, Lee YS (2011) Size controlled synthesis of Li_2MnSiO_4 nanoparticles: effect of calcination temperature and carbon content for high performance lithium batteries. J Colloid Interface Sci 355(2):472–477
32. Aravindan V, Karthikeyan K, Kang KS, Yoon WS, Kim WS, Lee YS (2011) Influence of carbon towards improved lithium storage properties of Li_2MnSiO_4 cathodes. J Mater Chem 21(8):2470–2475
33. Aravindan V, Karthikeyan K, Ravi S, Amaresh S, Kim WS, Lee YS (2010) Adipic acid assisted sol-gel synthesis of Li_2MnSiO_4 nanoparticles with improved lithium storage properties. J Mater Chem 20(35):7340–7343
34. Aravindan V, Karthikeyan K, Lee JW, Madhavi S, Lee YS (2011) Synthesis and improved electrochemical properties of Li_2MnSiO_4 cathodes. J Phys D 44(15):152001
35. Yin SC, Grondey H, Strobel P, Anne M, Nazar LF (2003) Electrochemical property: structure relationships in monoclinic $Li_{3-y}V_2(PO_4)_3$. J Am Chem Soc 125(34):10402–10411. doi:10.1021/ja034565h
36. Huang H, Yin SC, Kerr T, Taylor N, Nazar LF (2002) Nanostructured composites: a high capacity, fast rate $Li_3V_2(PO_4)_3$/carbon cathode for rechargeable Lithium batteries. Adv Mater 14(21):1525–1528. doi:10.1002/1521-4095
37. Patoux S, Wurm C, Morcrette M, Rousse G, Masquelier C (2003) A comparative structural and electrochemical study of monoclinic $Li_3Fe_2(PO_4)_3$ and $Li_3V_2(PO_4)_3$. J Power Sources 119–121:278–284. doi:10.1016/s0378-7753(03)00150-2
38. Zaghib K, Goodenough JB, Mauger A, Julien C (2009) Unsupported claims of ultrafast charging of $LiFePO_4$ Li-ion batteries. J Power Sources 194(2):1021–1023. doi:10.1016/j.jpowsour.2009.05.043
39. Yang S, Song H, Chen X (2006) Electrochemical performance of expanded mesocarbon microbeads as anode material for lithium-ion batteries. Electrochem Commun 8(1):137–142. doi:10.1016/j.elecom.2005.10.035